Journal of Materials Chemistry C

Accepted Manuscript

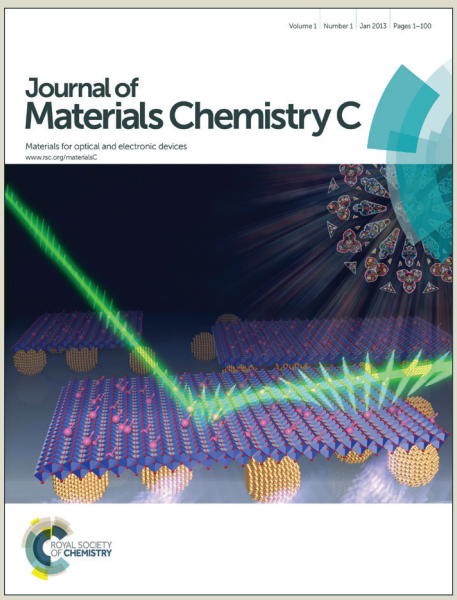

ROYAL SOCIETY OF CHEMISTRY

www.rsc.org/materialsC

High thermoelectric performance of Nb-doped $SrTiO_3$ bulk materials with different doping levels

Boyu Zhang,[a] Jun Wang,*[a] Tao Zou,[b] Shuai Zhang,*[c] Xinba Yaer,[a] Nan Ding,[a] Chengyan Liu,*[d] Lei Miao,[d] Yan Li[a] and Yin Wu[a]

[a] School of Materials Science and Engineering, No. 49 Ai Min Road, Xin Cheng Qu, Inner Mongolia University of Technology, Hohhot, Inner Mongolia Autonomous Region 010051, P.R. China

[b] Beijing Center for Physical & Chemical Analysis, No. 27 Xi Sanhuan Road, Haidian District, Beijing 100089 P.R. China

[c] Department of Physics, Kent State University, Kent, Ohio 44242, USA

[d] Guangxi Key Laboratory of Information Material, Guangxi Collaborative Innovation Center of Structure and Property for New Energy and Materials, School of Material Science and Engineering, Guilin University of Electronic Technology, Guilin, 541004, P. R. China

Abstract

Nb-doped $SrTiO_3$ bulk materials with high quality are fabricated using a facile process. The doping level in $SrTiO_3$ is controlled in a doping range of 0-20 mol%. Thermoelectric response including electrical conductivity σ, Seebeck coefficient S, and thermal conductivity k has been investigated in high-temperature regime above 300 K. The ZT values show obvious doping-level dependences, in which the largest value as high as 0.37 at 1000 K and 0.40 at 1100 K is realized in the optimized doping range of 10-15 mol%. This is the first time such a remarkable thermoelectric performance was accomplished in electron-doped $SrTiO_3$ ceramics.

*Corresponding authors. Tel: +86-18847143759; Fax: +86 471 6575752.

E-mail: wangjun@imut.edu.cn (Jun Wang), shuaizh14@gmail.com (Shuai Zhang) and liucy@ms.giec.ac.cn (Chengyan Liu)

1. Introduction

Performance in thermoelectric (TE) materials is determined using the thermoelectric figure-of-merit Z with definition $ZT = S^2\sigma T/k$, where S, σ, and k represent the Seebeck coefficient, electrical conductivity and thermal conductivity, respectively. To gain a high performance in TE material, efforts have been paid on increasing the so-called power factor (PF = $S^2\sigma$) as well as decreasing the thermal conductivity. S and σ are coupled via the charge carrier concentration: a high charge carrier concentration usually increases σ but decreases S. It is essential to find a balance point to achieve a large value of PF. A way to increase S is to increase the effective mass m^* of carrier as typically observed in 4f heavy-Fermion system [1], in which the strong electrons correlation results in the enhancement of m^* [2]. However, the carrier with heavy m^* will move slowly and therefore in turn leads to a low σ due to the small mobility. On the other hand, k can be effectively suppressed by introduction of nanostructure [3] and second phase [4] which can enhance phonon scattering at grain boundaries.

Because of the good stability at high temperatures, TE oxides have shown considerable potential as high-temperature TE materials. Corresponding to the large ZT value observed in p-type oxide semiconductor $NaCo_2O_4$ [5], extensive researches have been carried out on one promising candidate of n-type oxide insulator $SrTiO_3$ (STO), which shows direct band gap energy of 3.75 eV [6] with very low σ. The valence and conduction bands in $SrTiO_3$ correspond to the bands composed of O 2p state and Ti 3d-t_{2g} state, respectively. To enhance σ, foreign atomic doping is generally adopted. For example, Dehkordi et al [7] reported that Pr-doped $SrTiO_3$ ceramics show improved carrier mobility, and then a recorded ZT of 0.35 at 500 ^oC was obtained. Besides, other common elements are also selected to effectively optimize the

electrical properties, such as Nb and La [8, 9]. Upon doping Nb on Ti site, additional electrons can be induced by the replacement of Ti^{4+} with Nb^{5+} in $SrTiO_3$. In previous studies, Nb-doped STO epitaxial film exhibited high *ZT* value of ~0.37 and large PF value of 1.5 mW $m^{-1}K^{-2}$ at 1000 K [8], and a *ZT*~2.4 at room temperature was also estimated for a high-density two-dimensional electron gas confined within a unit cell layer thickness in STO, which is the highest value reported on STO materials [10]. However, carrier-doped STO bulk materials could not show comparable TE performance. For example, *ZT* of La-doped STO bulk single crystal was found to be as low as 0.06 at room temperature, although its large PF value of 2.8-3.6 mW $m^{-1}K^{-2}$ that is comparable to that of Bi_2Te_3. It is because of a high thermal conductivity (k > 90 mW/K cm) [9].

Very recently, several research groups have reported an enhanced *ZT* in nano-structured bulk alloy material such as BiSbTe [11] and PbTe [12] upon reduction in thermal conductivity. This strategy was also successfully applied on STO based TE ceramics [13, 14], in which nano-structured $La_xSr_{1-x}TiO_3$ shows a *ZT* = 0.37 at 973 K with low k. To the best of our knowledge, this is the largest value ever obtained in STO-based bulk materials. However, due to some technical problems on synthesis of nano-particles, an enhanced *ZT* has not been realized in Nb-doped STO yet, in spite that the *ZT* was improved upon the introduction of additional nano-wires [4] and nano-inclusions [15] to the carrier doped STO system. In this paper, rather than solid-state reaction [16, 17] or molten salt synthesis method [14] well used in previous studies, we design a facile process to prepare Nb doped STO (Nb-STO) bulk samples within micro-size grains. Note that this approach is not only simple and low cost, but can also be employed to prepare large-scaled ceramic TE materials. More importantly, to the best of our

knowledge, the *ZT* observed in our materials is as high as 0.40 at 1100 K, which is the highest value obtained in electron-doped STO bulk materials.

2. Experimental

Samples of STO doped with 0 mol%, 5 mol%, 10 mol%, 15 mol% and 20 mol% Nb were prepared by a hydrothermal method using tetrabutyltitanate [$Ti(OBu)_4$], strontium nitrate [$Sr(NO_3)_2$], sodium hydroxide NaOH, ethylene glycol, and Niobium pentahloride ($NbCl_5$). In a typical synthesis process, to obtain a doping level of 20 mol%, 8 mmol of $Ti(OBu)_4$ and 2 mmol of $NbCl_5$ were dissolved in 30 mL of ethylene glycol, followed by adding 6.4 mol/L NaOH. Then, 10 mmol of $Sr(NO_3)_2$ were dissolved in 15 mL of deionized water. The two solutions were mixed together to obtain a microemulsion, which was immediately transferred to a 100 mL Teflon lined stainless-steel autoclave and kept at 180 ^oC for 24 hours. To remove the byproduct, the obtained powders were washed with diluted acetic acid, which is followed by deionized-water washing. The final products were dried at 60 ^oC. The dried powders were preformed into disk under 4 Mpa, and further pressed by Cold Isostatic Pressing (CIP) under 250 Mpa. The samples were then embedded into carbon powder placed in corundum crucibles and sintered at 1300 ^oC for 5 hours in a muffle furnace, during which oxygen vacancy should generate to contribute excess electrons, so that the electrical conductivity of n-type $SrTiO_3$ would be further enhanced [18]. All the specimens were characterized by the scanning electron microscopy (SEM), X-ray diffraction (XRD), and transition electron microscope (TEM). The SEM images results were collected on a FEI Quanta FEG-650 scanning electron microscope. The powder XRD patterns and TEM images were obtained using Rigaku D/Max-25000 diffractometer and FEI Tecnai G^2 F20S-TWIN, respectively. Electrical conductivity and

Seebeck coefficient were measured from 300 to 1100 K under helium atmosphere using thermoelectric apparatus (LSR-3, Linseis Germany). Thermal conductivity was calculated using thermal diffusivity, specific heat, and density. Thermal diffusivity was measured by a laser flash analysis (LFA 457, Netzsch). The specific heat was measured by differential scanning calorimeter (DSC, STA 449F3, Netzsch, Germany)

3. Results and discussion

Figure 1a shows XRD patterns of hydrothermally synthesized 5 mol%, 10 mol%, 15 mol% and 20 mol% Nb doped STO together with pure STO. The Nb-STO samples obtained in the present study show high quality with single phase of cubic perovskite structure, which is comparable with pure STO. The slightly broadened diffraction peak implies that the particle size is significantly small. The diffraction angle decreases with increasing lattice constants, e.g., [110] peak shifts to lower diffraction angles monotonically with increasing doping up to 20 mol% as shown in Fig. 1b. In the meanwhile, the unit-cell volumes estimated from XRD data increase with doping level. Such an increase in cell volume is related to the replacement of small-sized Ti^{4+} ions (60.5 pm) in the *B* site of the perovskite structure with the larger Nb^{5+} ions (64.0 pm). Note that the single-phase XRD patterns and the linear doping dependence of unit-cell volume clearly suggest the bulk nature of carrier-doped STO with actually controlled doping levels.

In XRD patterns of as-sintered samples as shown in Fig. 1d, some unexpected weak peaks are found around $2\theta = 28$ and 35 degree, implying the presence of second rutile phase (TiO_2 or Nb-doped TiO_2). According to the defect chemistry model, the donor compensation mechanism should shift from the cation vacancy to the electronic type [19]. Thus, a possible

mechanism of the precipitation to form a second phase at low oxygen partial pressure and high temperature may take place as [20],

$$Sr_{1-\frac{x}{2}}Ti_{1-x}Nb_xO_3 \rightarrow Sr_{1-\frac{x}{2}}Ti_{1-x-y}Nb_{x-y}O_{3-4y} + yTiO_2 + yNbO_2 \quad , \qquad (1)$$

where $y<x\leq 0.2$.

In Figure 2a and b, we display the SEM image and high-resolution TEM (HRTEM) image of 15 mol% Nb-doped powder samples. The SEM images for Nb-STO disk samples with different doping level are shown in Fig. 2c-f. These images demonstrate the obtained nano-size particle with different doping levels is as large as up to 20 nm with an average size of ~10 nm. The HRTEM image shows that the lattice fringes of typical (110) facets is 0.278 nm, which is slightly larger than that of pure STO (0.275 nm). This also supports the increase of unit-cell volume upon replacement of small-size Ti^{4+} ion with large Nb^{5+} ion as previously discussed. Moreover, the HRTEM image confirms again that the nano-particle contains several nano-grains (> 5 nm) in different orientation (Fig. 2b). Besides the [110] peak, some other diffraction peaks of [111], [200], [211], and [310] peaks are also observed in electron diffraction (Fig. 2b inset), which suggests the presence of grains with different orientation in nano particles. On the other hand, the SEM images for sintered samples (Fig. 2c-f) show that the bulk samples even contain micro-scale crystals, indicating that a significant grain growth occurs in sintering process. This corresponds to the sharp diffraction peak observed in XRD results for as-sintered samples (Fig. 1d). More interestingly, one can see the clear growth steps on the crystal surface, which is likely to suggest that the growth mechanism may reduce interface scattering of electrons, enhance carrier mobility, and hence increase the electrical conductivity as discussed later [21, 22].

The electrical conductivity of un-doped STO samples is too small to measure that is not discussed hereinafter. The temperature dependence of electrical conductivity of Nb-doped STO samples is shown in Fig. 3a. σ(T) of all obtained samples have values in the range of 150-600 Scm^{-1} at all temperature and show a similar temperature dependence with a broad peak around 450 K, which is also observed in bulk La-doped STO samples with actual doping level of 9.0% by Park et al. [13]. Such a peak behavior is related to the semiconductor-like nature at low temperatures, suggesting that some excess electrons trend to be localized and can be thermally excited. This phenomenon may be due to the distortion of local structures [13] or the generation of second phase. When the temperature exceeds 450 K, the electron concentration should be temperature independent because all excess electrons are reasonably excited. As a result, the σ(T) decreases proportionally to $T^{-1.5}$ for all doping levels (Fig. 3a inset), which agree well with temperature dependencies of μ ($T^{-1.5}$) [23], indicating the phonon scattering plays a dominant role in carrier scattering mechanism. At a fixed temperature above 500 K, σ increases with increasing doping level due to the higher carrier concentration at higher doping level. Electrical conductivity show no clear difference for 15-20 mol%, which could be related the second phase in 20 mol% resulting in a similar carrier concentration as in 15 mol%. Furthermore, the presence of TiO_2 or Nb-doped TiO_2 can cause some restricting effect to σ as found in Y-doped STO polycrystalline samples [24].

Figure 3b shows the temperature dependence of the value of Seebeck coefficient, which increases with increasing temperature. Moreover, *S* decreases with increasing doping level of Nb (Fig 3b inset), which is in good agreement with the result of Ohta et al. [8]. Such a result is exactly opposite to the doping dependence of σ and can be explained by the model proposed

for metals or degenerate semiconductors [25].

$$S = \frac{8\pi^2 k_B^2}{3eh^2} m^* T \left(\frac{\pi}{3n}\right)^{\frac{2}{3}} , \qquad (2)$$

where k_B is Boltzmann constant, e is electronic charge, and n is the electron concentration of a doped semiconductor. The temperature and doping concentration dependence of S observed in our samples are in good agreement with other carrier doped STO materials [8, 13, 16, 23]. Usually, S depends on carrier concentration, effective mass of carrier, chemical potential, and Hall mobility [16]. In this study, samples with doping level of 5-15 mol% show larger S value compare with reported bulk STO materials (Fig. 3b), we consider the enhanced S obtained in bulk material in another possible mechanism, in which the growth steps on the crystal surface contributes to the improvement of S upon the introduction of meso-scale to micro-scale grain boundaries in the Nb-doped STO ceramics. A detailed study of the correlation between crystal growth and S will be the focus of future work. As can be seen in the definition of S (Eq. 2), the increase of carrier concentration can decrease Seebeck coefficient whereas a heavy effective mass m^* will correspondingly enhance the S value. The m^* appears to increase with increasing doping level, which could be mainly due to an increase in the lattice parameter or an increase in the distance between two neighboring Ti ions in the unit cell (Fig. 1c) as experimentally and theoretically found in carrier-doped STO system [8, 26]. The monotonic decrease of S with increasing doping level is consistent with the common understanding that the carrier concentration plays a dominant role in S rather than the contribution from slightly enhanced m^*.

Based on the measured S and σ, we show the temperature dependence of the calculated PF ($S^2\sigma$) in Fig. 3c. The rapid increase below 500 K is due to the peak found in $\sigma(T)$ that

corresponds to semiconductor-like nature. Interestingly, the PF above ~650 K is independent on temperature for doping level of 5, 15 and 20 mol%, while that for 10 mol% decreases slightly with increasing temperature from 600 to 1100 K. The PF value for 5 mol% in whole temperature range is rather lower than the other doping levels due to its considerably small electrical conductivity although the biggest *S* is obtained in this doping level. The maximum of PF value at the highest temperature (1100 K) is obtained as 1.15 mW/mK^2 in both 10 mol% and 15 mol%, which is even two times larger than the previously reported value in Nb-doped STO materials [15]. Such a huge enhancement is realized due to the improved Seebeck coefficient while electronic conductivity is kept in a comparable level. The PF values, however, are slightly smaller than the value at same doping level of the thin film published earlier [8], due to the fact that electrical conductivity of our bulk samples are smaller than that of the thin film resulting from the scattering of carriers by the second phase and grain boundary, in spite of our Seebeck coefficients are slightly larger than that of the thin film. On the other hand, grain boundaries are essential for the reduction of thermal conductivity in polycrystalline bulk materials.

The temperature dependence of thermal conductivity is shown in Fig. 3d. In general, the total thermal conductivity is composed with two independent components $k_{total} = k_e + k_L$, where k_e and k_L represent the contribution from electron and lattice, respectively. The k_e is estimated using the Wiedemann Franz law $k_e = LT\sigma$ where L is the Lorenz number (2.44×10^{-8} V^2 K^{-2}). The inset shows the obtained temperature dependence of k_L, which appears to play a dominant role in total thermal conductivity. With increasing the concentration of Nb, no obvious doping dependence was found in k_L of the doped STO system, implying again that

the lattice contribution is dominant rather than the changing carrier density in different doping levels as found in other electron doped STO materials. The total thermal conductivity observed in this study is in good agreement with results from Park *et al.* [13] and Kikuchi *et. al*.[27], and significantly smaller than that of single crystalline $SrTiO_3$ [9].

The *ZT* value calculated using the measured Seebeck coefficient, electrical and thermal conductivity is shown in Fig. 4. Due to the lack of some thermal conductivity measurement, k_{total} above 1000 K is estimated as the same as 1000 K and k_{total} for 5 mol% in whole range is considered to be the same as other doping levels. Such a conservative estimation will not affect our discussion on the value of *ZT*. For all doping levels, *ZT* increases with increasing temperature and reaches the values of 0.11, 0.37, 0.37 and 0.30 at 1000 K and the maximum values of 0.12, 0.40, 0.40 and 0.32 at 1100 K for 5, 10, 15 and 20 mol% Nb-doped samples, respectively, including the highest value ever observed in carrier doped STO system [13, 27, 28]. More importantly, note that the non-linear doping dependence of *ZT* value at 1000 K shows extreme similarity to that found in Nb-doped STO epitaxial film [8]. We reasonably conclude that the dome-like doping dependence of *ZT* reflects the nature in electron-doped STO, although the nominal doping level is used in our discussion.

Like *ZT*, the thermoelectric compatibility factor, $s = \left(\sqrt{1+ZT}-1\right)/(ST)$, is essential thermoelectric property for designing a thermoelectric device [29]. Therefore, the thermoelectric compatibility factors are calculated and their temperature dependences are shown in Fig. 4 inset. There are no obvious temperature dependences in thermoelectric compatibility factor above 500 K, which indicate present samples could be suitable for thermoelectric device.

4. Conclusion

In summary, we synthesized Nb-doped $SrTiO_3$ nano-particles with different doping level using a facile method. Bulk materials were obtained by a pressure-less sintering process. A remarkable thermoelectric performance with ZT= 0.40 (0.37) at 1100 K (1000 K) is realized on 10 and 15 mol% doping, which is the highest value found in carrier doped bulk STO materials. With increasing doping level, no apparent doping dependence of thermal conductivity was observed, while reasonable balance point between Seebeck coefficient and electrical conductivity appears to present in the most optimized doping level 10-15 mol%. Note that the synthesis of powders and preparation of bulk materials used in this study could be one potential candidate to be used for further TE application.

Acknowledgment

This work is partially supported by Science Research Grant for Inner Mongolia Higher Educational Institute to Jun Wang (NJZY12065) and open fund of Key laboratory for Guangzhou Institute of Energy Conversion, Chinese Academy of Sciences (GIEC) (y407k61001).

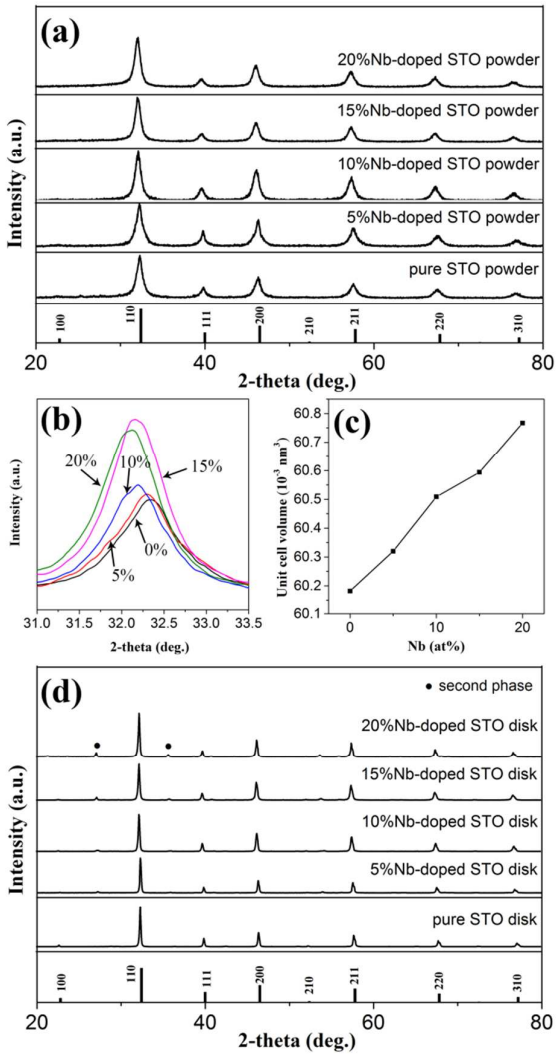

Fig.1 (a) X-ray diffraction patterns, (b) [110] diffraction peak of STO with different doping level of Nb, (c) Unit cell volume derived from the lattice parameter refinement plotted as a function of Nb content of powder samples synthesized from hydrolysis method and (d) X-ray diffraction patterns of disk samples.

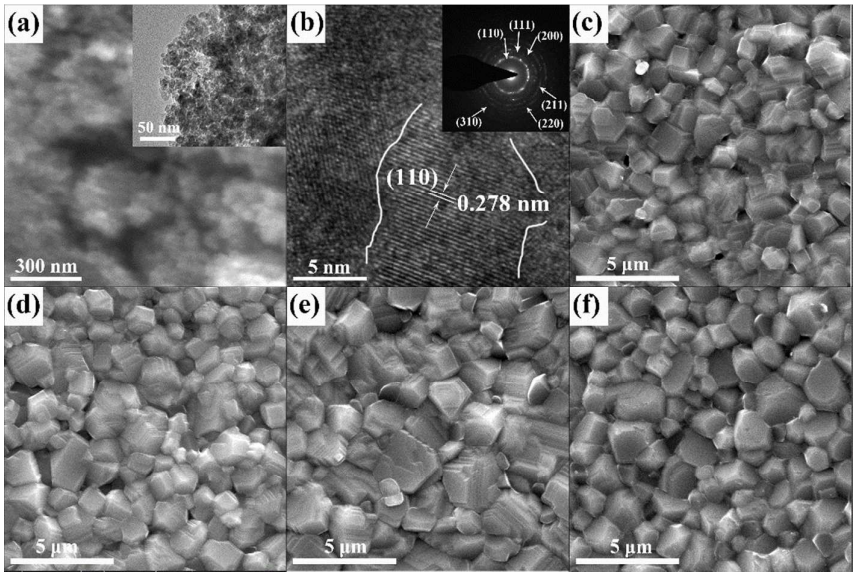

Fig. 2 (a) SEM image and the inset of TEM image, (b) HRTEM image and the inset of STO nanoparticles with 15% Nb doping concentration. SEM images of different doping concentration STO ceramics, (c) 5%, (d) 10%, (e) 15%, (f) 20%, respectively.

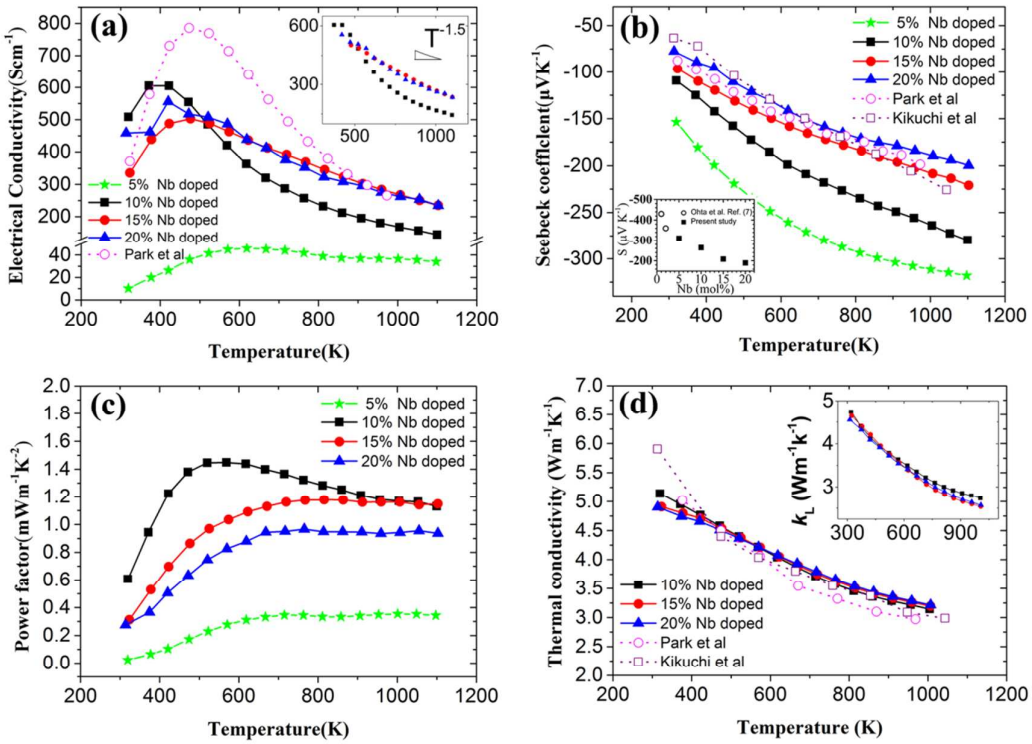

Fig. 3 Temperature dependence of (a) Electrical conductivity (σ), (b) Seebeck coefficient (S), (c) Power factor (PF) and (d) Total thermal conductivity and Lattice thermal conductivity. (a) inset, the σ decreasing proportionally with$T^{-1.5}$ from 473K to 1100K, (d) inset, The temperature dependence of lattice thermal conductivity.

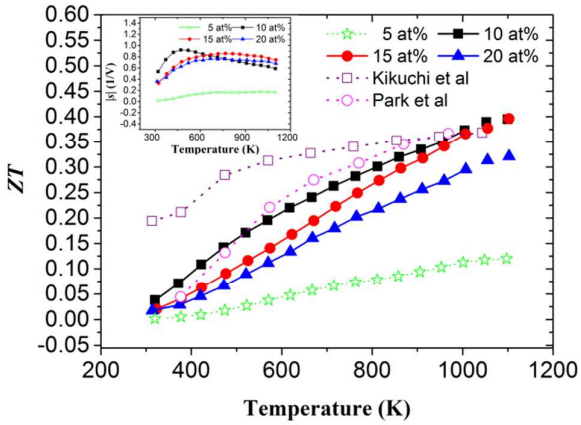

Fig.4 Temperature dependence of *ZT* and thermoelectric compatibility factors (inset) for Nb-doped STO samples with different Nb concentration

References

1. Mahan, G. D. Good Thermoelectrics. In *Solid State Physics*, Henry, E.; Frans, S., Eds. Academic Press: 1997; Vol. 51, pp 81-157.
2. Ando, Y.; Miyamoto, N.; Segawa, K.; Kawata, T.; Terasaki, I. Specific-heat evidence for strong electron correlations in the thermoelectric material $NaCo_2O_4$. *Physical Review B* **1999,** 60, 10580-10583.
3. Lan, Y.; Poudel, B.; Ma, Y.; Wang, D.; Dresselhaus, M. S.; Chen, G.; Ren, Z. Structure Study of Bulk Nanograined Thermoelectric Bismuth Antimony Telluride. *Nano Letters* **2009,** 9, 1419-1422.
4. Wang, N.; He, H. C.; Ba, Y. S.; Wan, C. L.; Koumoto, K. Thermoelectric properties of Nb-doped SrTiO3 ceramics enhanced by potassium titanate nanowires addition. *J. Ceram. Soc. Jpn.* **2010,** 118, 1098-1101.
5. Terasaki, I.; Sasago, Y.; Uchinokura, K. Large thermoelectric power in ${\mathrm{NaCo}}_{2}{\mathrm{O}}_{4}$ single crystals. *Physical Review B* **1997,** 56, R12685-R12687.
6. van Benthem, K.; Elsässer, C.; French, R. H. Bulk electronic structure of SrTiO3: Experiment and theory. *Journal of Applied Physics* **2001,** 90, 6156-6164.
7. Dehkordi, A. M.; Bhattacharya, S.; He, J.; Alshareef, H. N.; Tritt, T. M. Significant enhancement in thermoelectric properties of polycrystalline Pr-doped SrTiO3−δ ceramics originating from nonuniform distribution of Pr dopants. *Applied Physics Letters* **2014,** 104, 193902.
8. Ohta, S.; Nomura, T.; Ohta, H.; Hirano, M.; Hosono, H.; Koumoto, K. Large thermoelectric performance of heavily Nb-doped SrTiO3 epitaxial film at high temperature. *Applied Physics Letters* **2005,** 87, 092108.
9. Okuda, T.; Nakanishi, K.; Miyasaka, S.; Tokura, Y. Large thermoelectric response of metallic perovskites: Sr1-xLaxTiO3 (0 <= x <= 0.1). *Physical Review B* **2001,** 63.
10. Ohta, H.; Kim, S.; Mune, Y.; Mizoguchi, T.; Nomura, K.; Ohta, S.; Nomura, T.; Nakanishi, Y.; Ikuhara, Y.; Hirano, M.; Hosono, H.; Koumoto, K. Giant thermoelectric Seebeck coefficient of a two-dimensional electron gas in SrTiO3. *Nature materials* **2007,** 6, 129-34.
11. Poudel, B.; Hao, Q.; Ma, Y.; Lan, Y.; Minnich, A.; Yu, B.; Yan, X.; Wang, D.; Muto, A.; Vashaee, D.; Chen, X.; Liu, J.; Dresselhaus, M. S.; Chen, G.; Ren, Z. High-thermoelectric performance of

nanostructured bismuth antimony telluride bulk alloys. *Science* **2008,** 320, 634-8.

12. Biswas, K.; He, J.; Blum, I. D.; Wu, C. I.; Hogan, T. P.; Seidman, D. N.; Dravid, V. P.; Kanatzidis, M. G. High-performance bulk thermoelectrics with all-scale hierarchical architectures. *Nature* **2012,** 489, 414-8.

13. Park, K.; Son, J. S.; Woo, S. I.; Shin, K.; Oh, M.-W.; Park, S.-D.; Hyeon, T. Colloidal synthesis and thermoelectric properties of La-doped $SrTiO_3$ nanoparticles. *Journal of Materials Chemistry A* **2014,** 2, 4217.

14. Wang, J.; Ye, X.; Yaer, X.; Zhang, B.; Ma, W.; Miao, L. High thermoelectric performance of niobium-doped strontium titanate bulk material affected by all-scale grain boundary and inclusions. *Scripta Materialia* **2015,** 99, 25-28.

15. Wang, N.; Chen, H.; He, H.; Norimatsu, W.; Kusunoki, M.; Koumoto, K. Enhanced thermoelectric performance of Nb-doped SrTiO3 by nano-inclusion with low thermal conductivity. *Scientific reports* **2013,** 3, 3449.

16. Ohta, S.; Ohta, H.; Koumoto, K. Grain size dependence of thermoelectric performance of Nb-doped SrTiO3 polycrystals. *J. Ceram. Soc. Jpn.* **2006,** 114, 102-105.

17. Bochentyn, B.; Karczewski, J.; Gazda, M.; Jasiński, P.; Kusz, B. Interactions between components of SrTi0.98Nb0.02O3−δ-YSZ and SrTi0.98Nb0.02O3−δ-CeO2composites. *physica status solidi (a)* **2013,** 210, 538-545.

18. Kumar, S. R. S.; Barasheed, A. Z.; Alshareef, H. N. High Temperature Thermoelectric Properties of Strontium Titanate Thin Films with Oxygen Vacancy and Niobium Doping. *ACS Applied Materials & Interfaces* **2013,** 5, 7268-7273.

19. Kolodiazhnyi, T.; Petric, A. The Applicability of Sr-deficient n-type SrTiO3 for SOFC Anodes. *J Electroceram* **2005,** 15, 5-11.

20. Suthirakun, S.; Xiao, G.; Ammal, S. C.; Chen, F.; zur Loye, H.-C.; Heyden, A. Rational design of mixed ionic and electronic conducting perovskite oxides for solid oxide fuel cell anode materials: A case study for doped SrTiO3. *Journal of Power Sources* **2014,** 245, 875-885.

21. Wang, N.; Li, H.; Ba, Y.; Wang, Y.; Wan, C.; Fujinami, K.; Koumoto, K. Effects of YSZ Additions on Thermoelectric Properties of Nb-Doped Strontium Titanate. *Journal of Elec Materi* **2010,** 39, 1777-1781.

22. Shang, P.-P.; Zhang, B.-P.; Li, J.-F.; Ma, N. Effect of sintering temperature on thermoelectric properties of La-doped SrTiO3 ceramics prepared by sol–gel process and spark plasma sintering. *Solid State Sciences* **2010,** 12, 1341-1346.

23. Ohta, S.; Nomura, T.; Ohta, H.; Koumoto, K. High-temperature carrier transport and thermoelectric properties of heavily La- or Nb-doped SrTiO[sub 3] single crystals. *Journal of Applied Physics* **2005,** 97, 034106.

24. Ito, M.; Matsuda, T. Thermoelectric properties of non-doped and Y-doped SrTiO3 polycrystals synthesized by polymerized complex process and hot pressing. *Journal of Alloys and Compounds* **2009,** 477, 473-477.

25. Cutler, M.; Leavy, J. F.; Fitzpatrick, R. L. Electronic Transport in Semimetallic Cerium Sulfide. *Physical Review* **1964,** 133, A1143-A1152.

26. Wunderlich, W.; Ohta, S.; Ohta, H.; Koumoto, K. Effective mass and thermoelectric properties of SrTiO3-based natural superlattices evaluated by ab-initio calculations. *Thermoelectrics, 2005. ICT 2005. 24th International Conference on (IEEE, 2005)* **2005**, 252-255.

27. Kikuchi, A.; Okinaka, N.; Akiyama, T. A large thermoelectric figure of merit of La-doped SrTiO3

prepared by combustion synthesis with post-spark plasma sintering. *Scripta Materialia* **2010,** 63, 407-410.

28. Yaremchenko, A. A.; Populoh, S.; Patrício, S. G.; Macías, J.; Thiel, P.; Fagg, D. P.; Weidenkaff, A.; Frade, J. R.; Kovalevsky, A. V. Boosting Thermoelectric Performance by Controlled Defect Chemistry Engineering in Ta-Substituted Strontium Titanate. *Chemistry of Materials* **2015,** 27, 4995-5006.

29. Snyder, G. J.; Ursell, T. S. Thermoelectric efficiency and compatibility. *Physical review letters* **2003,** 91, 148301.